Korean J. Chem. Eng., **30**(5), 1097-1104 (2013)
DOI: 10.1007/s11814-013-0010-2

Simulation of computational fluid dynamics and comparison of cephalosporin C fermentation performance with different impeller combinations

Shengbing Duan*,†, Guoqiang Yuan, Yanli Zhao**, Weijia Ni*, Hongzhen Luo*, Zhongping Shi*, and Fan Liu***

*Key Laboratory of Industrial Biotechnology, Ministry of Education, School of Biotechnology, Jiangnan University, Wuxi, Jiangsu 214122, China
**CSPC Hebei Zhongrun Pharmaceutical Co., Ltd., Shijiazhuang, Hebei 050041, China
(*Received 4 July 2012 • accepted 23 January 2013*)

Abstract−Cephalosporin C (CPC) fermentation by *Acremonium chrysogenum* is an extremely high oxygen-consuming process and oxygen transfer rate in a bioreactor directly affects fermentation performance. In this study, fluid dynamics and oxygen transfer in a 7 L bioreactor with different impellers combinations were simulated by computational fluid dynamics (CFD) model. Based on the simulation results, two impeller combinations with higher oxygen transfer rate (K_La) were selected to conduct CPC fermentations, aiming at achieving high CPC concentration and low accumulation of major by-product, deacetoxycephalosporin (DAOC). It was found that an impeller combination with a higher K_La and moderate shear force is the prerequisite for efficient CPC production in a stirred bioreactor. The best impeller combination, which installed a six-bladed turbine and a four-pitched-blade turbine at bottom and upper layers but with a shortened impellers inter-distance, produced the highest CPC concentration of 35.77 g/L and lowest DAOC/CPC ratio of 0.5%.

Key words: *A. chrysogenum*, Antibiotic, Cephalosporin C Production, CFD, Shear Force

INTRODUCTION

Cephalosporin C (CPC) fermentation by filamentous *Acremonium chrysogenum* is an extremely high oxygen-consuming process. A large amount of oxygen is required for a few reactions in the main CPC synthesis route, where oxygen is used as either electron acceptor or as substrate for biosynthetic oxygenases [1]. The consecutive formations of the intermediates, penicillin N and deacetoxycephalosporin C (DAOC), as well as the relevant enzymatic catalysis, require a huge amount of oxygen [2]. Oxygen shortage leads to accumulation of the intermediate penicillin N and DAOC, which dramatically decreases CPC production [3-5]. Due to the high viscosity feature and complex rheological properties of CPC fermentation, oxygen supply and DO control are very difficult to deal with [6].

Several studies have been reported to the ways of enhancing efficiencies of oxygen utilization/supplies in CPC fermentation. Basch and Chiang found that high expression of expandase/hydroxylase gene by genetic engineering were able to significantly reduce the level of DAOC present in the broth compared to that of control strain [7]. *A. chrysogenum* expressing a fungi oxygen-binding heme protein (Vitreoscilla hemoglobin) was able to enhance CPC production dramatically [8]. As already known, improvement of oxygen mass transfer capability is another effective method to alleviate the oxygen shortage problem in fermentation processes. However, few studies are reported on the features of oxygen transfer and rheologies in CPC fermentation, and the relationship between shear force in a bioreactor and the relevant CPC productivity. In CPC production, mechanically stirred bioreactors with multiple-impellers and aeration are frequently used. Design and analysis of such kinds of bioreactor with multiple-impellers agitation and aeration are crucial to the achievement of CPC fermentation. For rational design of an agitation system with multiple-impellers, two important factors should be considered: volumetric mass (oxygen) transfer coefficient (K_La) and shear force [9]. For filamentous microorganisms producing products such as CPC, the optimal impeller combinations selected should provide a sufficient mass transfer rate but not cause serious shear force which results in mechanical damage to cells or cell growth [10]. Several studies have demonstrated the effects of mechanical forces on the morphology of filamentous microorganisms and the overall fermentation productivities. Metz et al. found that the length of the mycelial particles of *Penicillin chrysogenum* (*Pe. chrysogenum*) decreased with increasing power input per unit mass in a reactor, indicating that the increased agitation caused the hyphae to become shorter, thicker and highly branched [11]. High agitation rates reduced the agglomeration of *Pe. chrysogenum* hyphal elements and caused a reduction in both pellet diameters and the concentration of pellets in the work of Nielsen [12]. Smith et al. also observed a drop in penicillin productivity by *Pe. chrysogenum* and the reduced hyphal lengths when increasing agitation [13].

Computational fluid dynamics (CFD) is a useful tool in analysis of highly complex fluid flow in mechanically stirred reaction tanks. Using CFD tools, many preliminary investigation works regarding mass transfer and shear environment in different kinds of bioreactors would have been done [14-18]. In this work, the fluid dynamics, oxygen mass transfer coefficient, and the shear force, in a 7 L stirred bioreactor with six different impeller combinations were simulated and investigated using the CFD tool Fluent®. Based on the CFD simulation results, the 7 L bioreactor installing the two impel-

†To whom correspondence should be addressed.
E-mail: duansb_0001@yahoo.com.cn

ler combinations with optimal prediction in mass transfer rate, as well as the control impellers (the standard impeller combination set in the purchased bioreactor) was applied to implement CPC fermentations. The resulting simulation results of the complex flow field in the reactor, the physiological shapes of *A. chrysogenum* in CPC fermentation obtained in the bioreactor and the relationship between them were carefully investigated and discussed, to interpret/explore the ways of CPC fermentation optimization in a well-designed stirred bioreactor.

MATERIALS AND METHODS

1. Strain and Fermentation Media

Acremonium chrysogenum HC-3, an industrial CPC producing strain, supplied by Hebei Zhongrun Pharmaceutical Co. Ltd. was used in this study.

Seed medium contained (w/w): sucrose 3.5%, glucose 0.5%, corn steep liquor 3.1%, D,L-methionine 0.05%, $CaCO_3$ 0.5%, soybean oil 0.5%%. pH 6.5. Fermentation medium contained (w/w): cornstarch 3.5%, dextrin 7.0%, corn steep liquor (dry weight) 5.0%, D,L-methionine 0.6%, urea 0.3%, $(NH_4)_2SO_4$ 1.3%, $CaCO_3$ 1.0%, KH_2PO_4 0.9%, soybean oil 5.0%, α-amylase (20,000 U/mL) 0.02%, and trace element solution. pH 5.6. Feeding media (w/w) were soybean oil (purchased at local supermarket), 25% ammonia water and 20% $(NH_4)_2SO_4$ solution.

2. Fermentation Conditions

Seed cultures were carried out in 500 mL Erlenmeyer flasks containing 50 mL seed medium. The flasks were placed on a rotary shaking incubator at 240 rpm and 28 °C for 84 h. CPC fermentation was implemented in a 7 L mechanically stirred fermentor (BIOTECH-7BG, Baoxing Co. Ltd., China) equipped with on-line DO/pH measurement probes, with initial medium volume of 5 L and air aeration rate of 1.2 vvm throughout the fermentations. The inoculation amount in all CPC fermentations was 15% (v/v). The fermentation temperature was controlled at 28 °C in the first 50 h, then it was shifted to 25 °C. pH was maintained at a range of 5.5-5.6 by automatically adding either diluted H_2SO_4 solution or ammonia water. The agitation initiated at 300 rpm, and it was manually increased by an increment of 50 rpm when DO dropped down to a low level (20%). The electronic balances (JA1102, Haikang Instrument Co. Ltd., China) connected to an industrial computer via a multi-channels A/D-D/A converter (PCL-812PG, Advantech Co. Ltd., Taiwan) was used to on-line monitor soybean oil addition amounts by measuring the weight losses in the feeding reservoirs. The CO_2 and O_2 partial pressure in exhaust gas were on-line measured by a gas analyzer (LKM2000A, Lokas Co. Ltd., Korea). The exhaust gas data and DO/pH signals from the fermentor control cabinet were collected into the industrial computer via RS232; oxygen uptake rate (OUR) and CO_2 evolution rate (CER) were then calculated on-line by the standard calculation formula. Soybean oil feeding was with DO-Stat based methods via the multi-channels A/D-D/A converter, with the aid of the self-developed control programs (Visual Basic, Ver. 6.0).

3. Impeller Combinations Configuration in Bioreactor

Six different impeller combinations in the same bioreactor were simulated and experimentally analyzed in this study. The schematic diagrams of the impeller combinations are shown in Fig. 1. As shown in Fig. 1, impeller combination 1 located a six-bladed disk turbine (6-BDT) at bottom in the bioreactor and a four-pitched-blade turbine (4-PBT) at the upper layer. The same combination was applied for an impeller combination 2 except that the mounting position of the 6-BDT moved 15 mm upward. Impeller combination 3 featured with two 6-BDT, and impeller combination 4 had two 6-BDT located at the top and bottom of the agitation axis and a 4-PBT mounting at the middle. Impeller combination 5 had three 6-BDT, and impeller combination 6 featured with two 6-BDT (located at the middle and bottom) and one 4PBT (located at the top). The details of the impeller combinations including the impeller types/outlooks and its geometrical size, as well as the impeller's mounting positions are shown in Fig. 1, Table 1 and Table 2. Aeration was supplied through a thin gas pipe. The inlet vent of the pipe was perpendicular to the tank bottom facing downward, and it was located between the bottoms of the bioreactor and the agitation shaft.

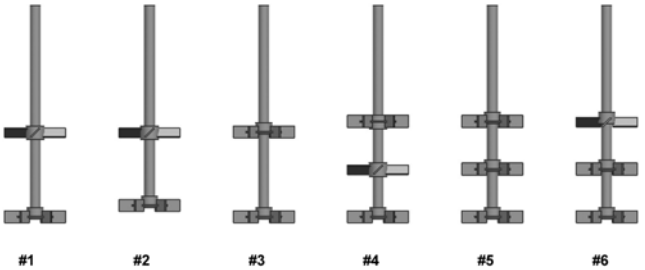

Fig. 1. Schematic diagram of six impellers combinations. Combination 1: one 6-BDT (located at the bottom of tank) and one 4-PBT (located at the top) with standard inter-distance between impellers; Combination 2: the same impellers combination as 1 but moving the mounting position of 6-BDT upward for 15 mm; Combination 3: two 6-BDTs with standard inter-distance between impellers; Combination 4: two 6-BDTs (located at the top and bottom) and one 4-PBT (located at middle); Combination 5: three standard 6-BDTs; combination 6: two 6-BDTs (located at the middle and bottom) and one 4-PBT (located at the top).

Table 1. Mounting position of the six impellers combinations

Impeller combinations	Distance from the bottom impeller to the bottom of tank/mm	Distance between impellers/mm
1	42	112
2	57	97
3	42	112
4	42	63
5	42	63
6	42	63

4. Analytical Methods

20 mL of fermentation broth was accurately taken at each sampling time. The samples were centrifuged at 8,000 rpm for 15 min. The supernatants were collected and properly stored for CPC, and DAOC measurements. The cell concentration was determined by cell dry weight analysis. Each cell pellet was washed twice with deionized water, and then dried at 105 °C until a constant weight was obtained. After properly diluting the supernatants, CPC and DAOC were measured by an Agilent 1200 HPLC, under the following conditions: reverse column ODS-C18 4.6 mm×250 mm;

Table 2. Main geometrical parameters of bioreactor and impellers

Bioreactor		Impellers	
Capacity/L	7	Six-bladed disk turbine size/mm	22×16
Filled volume/L	5	6BDT diameter/mm	80
Diameter/mm	171	Four-pitched-blade turbine size/mm	31×16
Liquid height/mm	231	4PBT diameter/mm	80
Baffle size/mm	225×13	Number of gas pipe inlet vent	17
Number of baffle	4	Gas pipe inlet vent diameter/mm	1

temperature 30 °C; flow rate 0.8 mL/min and mobile phase methanol/distilled water/phosphate=15/85/0.15 (v/v); detection at 254 nm with an UV detector. The standards of CPC and DAOC were supplied by CSPC Co. Ltd. The cell morphological shapes were visualized and recorded by an optical microscopy (Leica DM4000B Microscope) equipped with a photomicrographs and Image Pro 3.0 software, by suitably diluting the samples with distilled water. Rheological properties of the broth were tested using a programmable rotating rheometer (DV-III Ultra, Brookfield) with a Small Sample Adapter (SSA) and proper spindle, which provided a defined geometry system for accurate viscosity measurements of small sample volumes at precise shear rates. Less than 10 mL of broth was used for rheological test. The rheological test was done according to the method described by Marten et al. [19], and the recorded data of shear force and shear strain rate was correlated with power law model.

$$\tau = K\gamma^n \tag{1}$$

where τ, γ, K and n are shear force (Pa), shear strain rate (s^{-1}), consistency coefficient ($Pa \cdot s^n$) and flow index (dimensionless), respectively. The correlated parameters of n and K in this study could be formulated as n=0.75 and K=0.042 $Pa \cdot s^{0.75}$, which indicated that the fermentation broth belongs to shear thinning fluid.

5. CFD Model Set-up

To calculate the three-dimensional velocity and shear profiles in the bioreactor with six (6) different impeller combinations, each worked individually, a commercial CFD software code Fluent® (version 6.3.26, Fluent Inc., USA) was utilized to solve the Navier-Stokes equations. A lot of researchers have used this software to calculate flow field in stirred tanks [20,21]. GAMBIT® (version 2.3.16, Fluent Inc., USA) was used to generate mesh of the models. Multiple reference frames (MRF) method [22] was selected to set up the model in our case. Three or four parts of mesh were created for each model: the outer stationary part consisting of the stationary bulk of the tank including the baffles and two or three separated mesh parts containing each rotating impeller. Considering the geometrical complexity of the impellers, the element types used in all the three models were tetrahedral. Along with the Eulerian two-phase model, the dispersed multiphase k-ε turbulent model was also included to model the two phase turbulent flow in the stirred bioreactors. Aeration rate used was identical with that used the fermentations. According to the full baffled condition which assumes no vortex occurrence at the liquid surface, then the broth surface was set with degassing wall boundary, which only let gas escape from the surface and liquid bounded with no friction. Under these conditions, we assumed that the shaft (impellers) were set as a rotating wall of 400 rpm, all the other boundaries were set with rough wall boundaries, and the dispersed phase (gas phase) was air at 25 °C with uniform bubble diameter of 3 mm and without break-up/coalescence effects. To model the shear thinning property of the broth, a new liquid material was created in Fluent software. Viscosity of the new material was set as mutative variable of "visEqn" depending on the local shear strain rate in reactor using the Fluent Expression Language. The equation defining this variable is as follows:

$$\text{visEqn} = K\gamma^{n-1} \tag{2}$$

where n=0.71, K=0.032 $Pa \cdot s^{0.71}$ and γ was the built-in variable in the Fluent Solver. As the Solver could acquire the local shear strain rate, the apparent viscosity of the broth could be determined using the above equation. The CFD model was solved with Fluent® software (version 6.3.26, Fluent Inc., USA) installed in a Dawning 4000A supercomputer system (Dawning Information Industry Co. Ltd.). Eight AMD 248 processors and about 8GB available RAM were used to solve the CFD model. The converged steady state solution of the simulation was assumed when all the variable residuals decreased to a criterion level of 10^{-4}, and the total gas hold-up amount in the tank reached a constant level.

6. Oxygen Mass Transfer Coefficient Model

Based on Higbie's penetration theory, which is widely used to describe gas-liquid transfer, and the assumption of non-stationary diffusion of the elements in gas-liquid interface, Garcia-Ochoa and Gomez [23] proposed a theoretical model for predicting the oxygen mass transfer coefficient for shear thinning fluid as following.

$$K_L = \frac{2}{\sqrt{\pi}}\sqrt{D_L}\left(\frac{\varepsilon\rho}{K}\right)^{1/2(1+n)} \tag{3}$$

where D_L is the oxygen diffusivity in the liquid. K, n and ρ are the consistency coefficient, flow index and density of the fluid, respectively. ε is the local energy dissipation rate.

The specific area of bubble is determined by the following equation, where ϕ is the local volume fraction of the gas phase, and d_b is the mean diameter of the bubbles (3 mm).

$$a = \frac{6\phi}{d_b} \tag{4}$$

Based on this theoretical model, Garcia-Ochoa and Gomez predicted oxygen mass transfer coefficient in bioreactors with different scale under different operating conditions successfully. Therefore, the above two equations were used in this work to calculate the oxygen mass transfer coefficient. ε and ϕ in this work were obtained from the simulated results.

6. Shear Environment Calculation

Shear stress (shear force) everywhere in the fluid field can be cal-

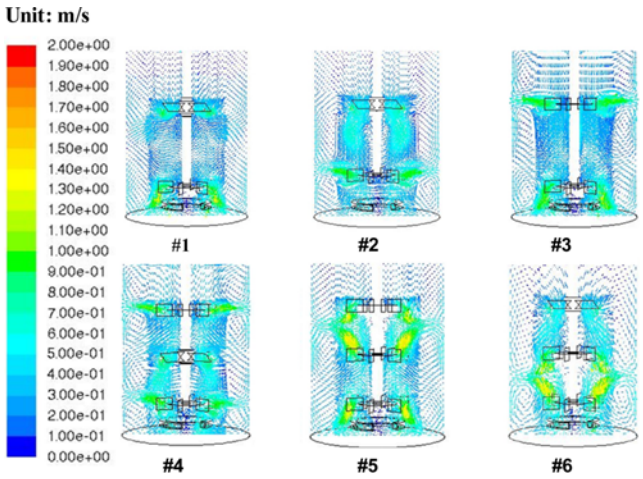

Fig. 2. Simulated velocity profiles of the six different impeller combinations. Color gradient represents the velocity magnitude, red denotes highest velocity and dark blue denotes the lowest velocity.

culated using Eq. (1). Based on a weighted average method embedded in Fluent® software (version 2.3.16, Fluent Inc., USA), the average shear strain rate could be calculated. Then, the average shear force was calculated by the apparent viscosity times average shear strain rate.

RESULTS AND DISCUSSION

1. The Simulation Results of Velocity Profile under Different Impeller Combinations

Simulation results of velocity profiles using the six impeller combinations (Fig. 2) indicated the flow patterns under different impeller combinations. Under impeller combination 1, 2 and 3, two flow circulations formed near the upper impeller and bottom impeller. With impeller combination 2, the radial flow appeared in the bottom of the reactor because the mounting position of the 6-BDT impeller was moved upward for 15 mm (as compared with that of combination 1). However, with impeller combination 3, radial flow formed near the upper region of the reactor. As for combination 1, no radial flow regions were observed inside the tank. In combination 1 and 3, the clearance between the two impellers was larger than their diameter, the discharge flow patterns developed by the upper and bottom impellers were almost independent. In contrast, a whole mixing flow pattern was formed with the combination 2. In the reactor installing the impellers (combination 4), two radial flow circulations formed in the areas close to the upper and bottom impellers, while an axial flow circulation appeared in the region nearby the middle 4-PBT impeller. The flow pattern obtained with combination 5 was somewhat similar to that of combination 1 because the flow circulations formed by the upper and middle impellers almost merged together, but the flow velocity in this case was fast. The flow pattern with impeller combination 6 was basically identical to that of using combination 2, as flow circulations produced by the middle and bottom impellers were merged to form a radial flow circulation.

The radial flow at the bottom of a bioreactor is crucial to fermentation performance. The existence of the bottom radial flow would improve the characteristics of oxygen supplies and distribution, because the breakage and dispersion of air bubbles could be enhanced, while at the same time, the blending time and area of air in liquid phase could be enlarged [24,25]. As shown in Fig. 2, with the impeller combination 1, 3 and 5, radial flows at the bottom of a stirred tank were not formed; this fact suggested that those three combinations are not appropriate for the extensive oxygen-consuming fermentations such as CPC production.

In aerated fermentation broth, each flow circulation is an independent mixing area, and oxygen transfer rate is high within a flow circulation region. However, oxygen transfer between each individual flow circulation regions is low. Abrardi et al. [26] and Ahmed et al. [27] reported that the entire mixing performance of a reactor is dominated by the flow exchange rate between the adjacent circulations. By summarizing the above-mentioned results, excessive flow circulations are harmful to CPC fermentation due to a longer mixing/diffusing time of oxygen in a liquid medium. Impeller combination 4 formed excessive/complicated flow circulations leading to a low oxygen transfer; therefore, this impeller combination (4) is also not suitable for CPC fermentation and it could be withdrawn from the candidates list. At this stage, only two impeller combinations, namely combination 2 and 6 are still left in the optimal impellers combination category, and thus the investigation in the sequential sections was mainly focused on these two combinations.

2. Oxygen Mass Transfer Coefficient under Different Impeller Combinations

Fluent® software could calculate the velocity field. Based on the velocity field obtained, the energy dissipation distribution and local air volume fraction in the flow field were calculated. These data were then used to calculate average K_La in the tank by the theoretical models (Eqs. (3) and (4)). The simulation results of K_La of all of 6 impeller combinations are shown in Fig. 3. Fig. 3 shows that the oxygen transfer rate of combination 2 and 6 was higher than that of other combinations. K_La of combination 6 was the highest among the six combinations. It should be noted that a reactor with more impellers (1, 2 and 3: 2; 4, 5 and 6: 3) would consume more power when they are operated under the same agitation rate. In this study, we did not consider the index of power number as power con-

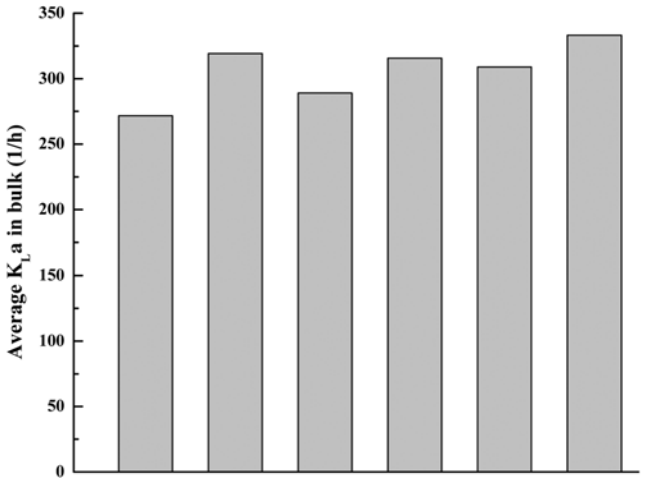

Fig. 3. Comparison of average oxygen mass transfer coefficients in the tank with six different impeller combinations.

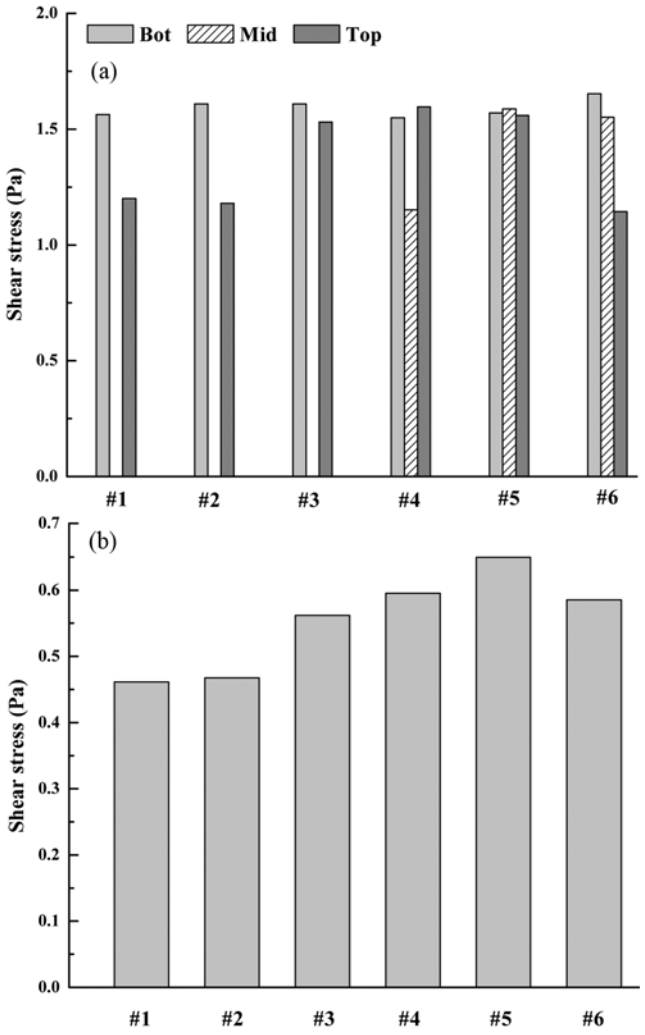

Fig. 4. Comparison of shear forces in the tank with the six different impeller combinations. (a) Local average shear strain rate at each impeller sweeping zone; (b) average shear strain rate in the liquid bulk.

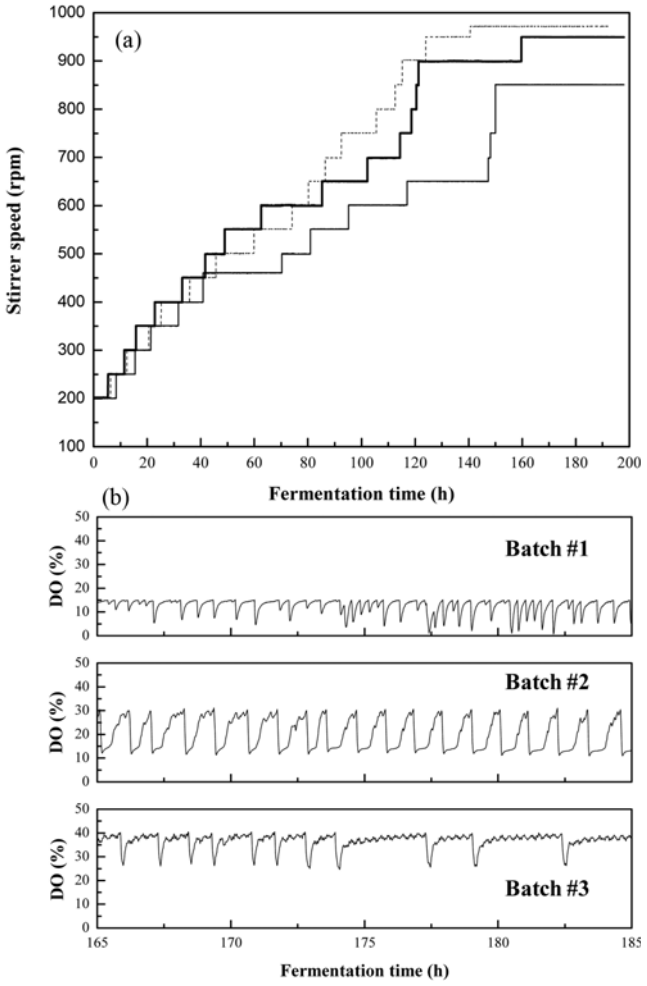

Fig. 5. Time courses of agitation rate and DO in different fermentation batches. Broken lines: fermentation batch I, bold solid lines: batch II, thin solid lines: batch III.

sumed in a lab-scaled bioreactor is difficult to measure.

3. Shear Environment under Different Impeller Combinations

The simulation results of the shear strain rates obtained with the six impeller combinations (Fig. 4) showed that the average shear force in combinations of 1 and 2 was about 0.46 Pa and the lowest among the six combinations. The average shear force in a reactor having three impellers was higher than that when two impellers were installed. It was observed that the maximum shear force was located at the impeller sweeping zone, and this force was much larger than the mean shear force in the liquid bulk. The results also showed that same type of impeller produced similar shear force at the sweeping zone. One 4-PBT impeller produced lower shear force (about 1.2 Pa) than that produced by one 6-BDT (about 1.6 Pa).

4. Fermentation Results Using Optimally Design Impellers Combinations

From the simulation results (Figs. 2, 3 and 4), it could be concluded that the highest K_La and the lowest shear force were obtained under impeller combination 6 and combination 2, respectively. High oxygen transfer rate reflected by a high K_La is favorable for CPC production, while a lower shear force but with comparably high K_La might be more promising because it supplies both higher oxygen transfer and mild shear environments to CPC fermentation. Here, as a result, we adopted combinations 2 and 6 as the optimal design impeller combinations to conduct CPC fermentations to see their practical and experimental effects, with combination 1 as the control or comparison base. Fermentations using combinations 1, 2 and 6 were referred as batch I, II and III, respectively, in the sequential section.

The agitation rates plotted in Fig. 5(a) indicated that agitation rate in batch III was much lower than that of I and II, suggesting that impeller combination 6 could minimize the agitation required for a normal CPC fermentation. On the other hand, as shown in Fig. 5(b), DO levels during main CPC production phase in batch II and III were much higher than that of batch I, even though a relatively mild agitation was applied for the former two cases. This fact demonstrated that the high oxygen transfer rates using impellers combinations 2 and 6 were beneficial for DO control and reducing the fermentation cost.

Fig. 6(a) plotted the soybean oil feeding curves in batch I, II and III. In batch I, only about 164 g of soybean oil was added, which

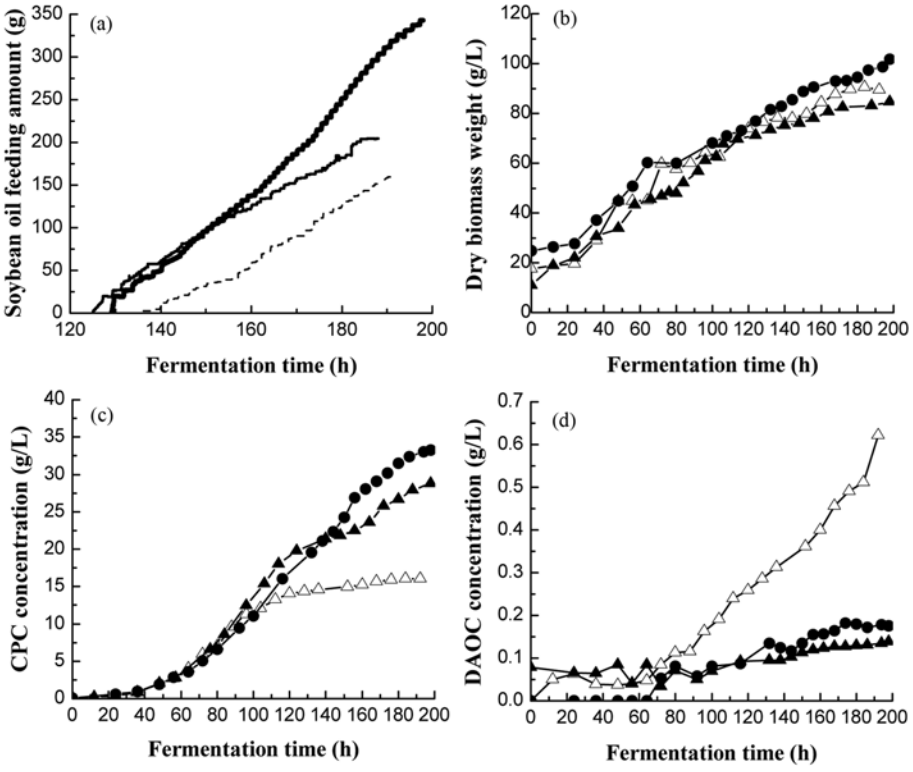

Fig. 6. Fermentation curves when using different impeller combinations. Broken lines and open triangles: fermentation batch I; bold solid lines and solid circles: batch II, thin solid lines and solid triangles: batch III. DO-Stat based feeding strategy was applied for soybean oil addition for the three batches.

was the lowest among the three batches. In batches I-III, soybean oil was fed with DO-Stat based feeding strategy. The very low level of DO in batch I was caused by the lower oxygen transferability (K_La) when using the impeller combination 1 (agitation had reached the highest level of 980 rpm), and the lower K_La limited the soybean oil feeding leading to a lower CPC concentration in turn. We defined soybean oil feeding rate in Fig. 6(a) in a shape of total soybean addition amount, and the slopes of the curves with regards to fermentation time could be recognized as the relevant soybean oil feeding rates. Soybean oil feeding rate in batch II was the highest, since impeller combination 2 supplied higher oxygen transfer and mild shear environments simultaneously. It should be addressed that overfeeding soybean oil could also lead to a very low DO level and thus deteriorate the overall CPC fermentation performance. Tollnick et al. [28] reported that the existence of a large amount of soybean oil and fatty acids (high level of soybean oil) would cause the formation of a highly viscous emulsion. The emulsion would make oxygen transfer difficult in fermentation broth, leading to a very low DO level and uncontrollability in DO.

In CPC fermentation, the major by-product, deacetoxycephalosporin C (DAOC), could accumulate up to a level of 1-2% DAOC/CPC (w/w) [29]. DAOC has similar molecular weight and structure as that of CPC. Separation of the two substances is very difficult, so that repressing DAOC accumulation during CPC fermentation has become the only way to control the quality of CPC fermentation product [30]. According to the investigations by Tollnick, the main factor accounting for DAOC accumulation is oxygen shortage, so that the best way to reduce DAOC accumulation is to avoid oxygen limitation [28]. As showed in Fig. 6(d), by adopting the optimally design impeller combinations, DAOC accumulation amount in batch II and III decreased dramatically as compared with that of batch I.

As shown in Fig. 6(c), CPC concentration in batch I ended at a level of 16 g/L, that was the lowest among the three batches. The low CPC concentration in this case was apparently due to the oxygen limitation during main CPC production phase. However, away from our expectation, both CPC concentration and dry biomass weight in batch III (with impellers combination 6) were lower than those of batch II. In addition, dry biomass weight in batch III was the lowest among the three batches (Fig. 6(b)). The above results were in conflict with the simulation results which indicated that combination 6 had the highest K_La. In general, an efficient CPC production relies on not only a high K_La but also lower/mild shear stress rate environment. The impeller combination selected should satisfy the requirements on both high oxygen transfer rate and mild shear force, as extremely high shear force may damage cells growth in the cultivations of microorganism such as *A. chrysogenum*. The simulation results shown in Fig. 4 demonstrated that combination 6 had the highest shear stress rate. Many studies have reported that high shear force led to deteriorated metabolites productivity when using filamentous microorganisms [11-13]. In the case of CPC production by *A. chrysogenum*, it was speculated that the high shear force when using impellers combination 6 severely damaged the cells structures and therefore their growth.

Fig. 7 shows that the rates of CPC synthesis and cell growth during main CPC production phase in batch I were extremely low due to oxygen limitation. In batch III, rates of CPC synthesis and cell growth

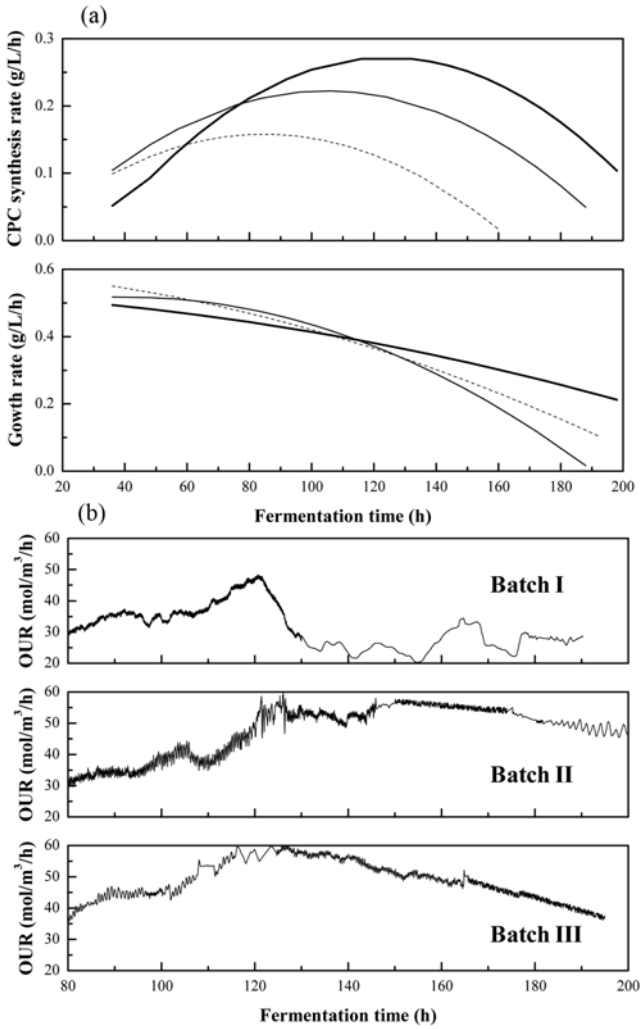

Fig. 7. Time courses of growth rate, CPC synthesis rate and OUR in different fermentation batches. Broken lines: fermentation batch I; bold solid lines: batch II; thin solid line: batch III.

were higher than that of batch II in the first 80-120 h. However, rates of CPC synthesis and cell growth declined quickly after that, and both rates reduced to the levels which were lower than those of batch II after 120 h. The changing patterns in oxygen uptake rate (OUR) also coincided with the above results. The average OUR in batch I was the lowest, particularly during the main CPC production phase, which again indicated that the low DO level in this case was due to the low oxygen transfer rate. The average OUR in batch II was the highest and very stable during the main CPC production phase. The average OUR in batch III was also high, but it declined gradually after 130 h. This declined feature in OUR actually reflected that the cell damage effects as they were subject to high shear force environment for long time.

CPC fermentation by *A. chrysogenum* is characterized by the feature of morphological differentiation [31]. According to Matsumura and Basak, the maximum CPC production rate coincides with the differentiation of filamentous hyphae to wide-highly swollen and metabolically active hyphal fragments [32,33]. Fig. 8 showed the morphological shapes of *A. chrysogenum* of the three batches at 48 h, 120 h and 168 h, respectively. Before 48 h, cells in all batches

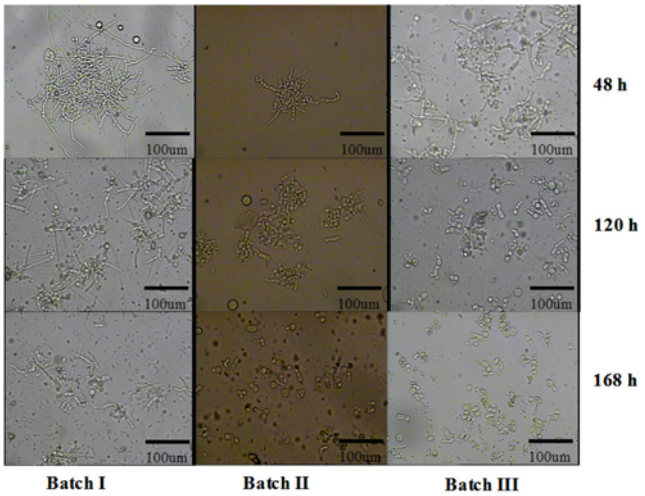

Fig. 8. Morphological shapes of *A. chrysogenum* HC-3 in three fermentation batches at different fermentation instant.

kept the shape of long-slender-smooth hyphae without differentiation. At 120 h, cells shape showed notable differences in the three batches. In batch I, some cells transformed to moderate swollen hyphal, but some others still kept the shape of long-slender-smooth hyphae; in batch II, cells successfully split into highly swollen hyphal fragments at this moment; but in batch III, almost all cells differentiated into arthrospores. At 168 h, some cells with long-slender-smooth hyphae shape could still be observed in batch I, while all of the cells differentiated into arthrospores in batches II and III. The early morphological differentiation into arthrospores shape at 120 h in batch III caused the decreases in cells metabolic and CPC synthetic capabilities, and the high shear force in batch III (combination 6) was responsible for the early morphological shape's shift and the resulting lower CPC synthesis rate.

CONCLUSION

Fluid dynamics and oxygen transfer in a 7 L bioreactor with different impeller combinations of six-bladed disk turbine (6-BDT) and four-pitched-blade turbine (4-PBT) were firstly simulated and investigated by computational fluid dynamics (CFD) model. Based on the simulation results, two impeller combinations with higher oxygen transfer effect were selected to conduct CPC fermentations, aiming at achieving high CPC concentration and low accumulation of DAOC. The major conclusions of this study could be summarized as below: 1) Both oxygen transfer capacity and shear stress environment in a stirred bioreactor are the extremely important factors affecting cell growth, carbon metabolism, as well as CPC synthesis. An impeller combination with a higher K_La and moderate shear force is the prerequisite for efficient CPC production in a stirred bioreactor. 2) Impeller combination 2, installed a 6-BDT and a 4-PBT impeller at bottom and upper layers but with a shortened inter-distance between the impellers, produced the highest CPC concentration of 35.77 g/L and lowest DAOC/CPC ratio of 0.5%.

ACKNOWLEDGEMENTS

The authors would like to express gratitude to the National Sci-

ence & Technology Supporting Program (2007BAI26B02) and Major State Basic Research Development Program (2007CB714303), of China for the financial assistance.

REFERENCES

1. J. Kozma and L. Karaffa, *J. Biotechnol.*, **48**, 59 (1996).
2. P. Hilgendorf, H. Diekmann, V. Heiser and M. Thoma, *Appl. Microbiol. Biotechnol.*, **27**, 247 (1987).
3. M. J. Rollins, S. E. Jensen, S. Wolfe and D. W. Westlake, *Enzyme Microb. Technol.*, **12**, 40 (1990).
4. W. Zhou, K. Holzhauer-Rieger, M. Dors and K. Schugerl, *Enzyme Microbiol. Technol.*, **14**, 848 (1992).
5. A. Yang, H. L. Dong and G. Liu, *J. Ind. Microbiol. Biotechnol.*, **39**, 269 (2012).
6. P. Mishra, P. Srivastava and S. Kundu, *World J. Microbiol. Biotechnol.*, **21**, 525 (2005).
7. J. Basch and S. J. Chiang, *J. Ind. Microbiol. Biotechnol.*, **20**, 344 (1998).
8. J. A. DeMondena, S. Gutiérrez, J. Velasco, F. J. Fernández, R. A. Fachini, J. L. Galazzo, D. E. Hughes and J. F. Martin, *Biotechnol.*, **11**, 926 (1993).
9. A. W. Nienow, *Appl. Mech. Rev.*, **51**, 3 (1998).
10. M. Papagianni, *Biotechnol. Adv.*, **22**, 189 (2004).
11. B. Metz, E. W. deBruijn and J. C. van Suijdam, *Biotechnol. Bioeng.*, **23**, 149 (1981).
12. J. Nielsen, C. L. Johansen, M. Jacobsen, P. Krabben and J. Villadsen, *Biotechnol. Prog.*, **11**, 93 (1995).
13. J. J. Smith, M. D. Lilly and R. I. Fox, *Biotechnol. Bioeng.*, **35**, 11 (1990).
14. M. Rahimi, A. Kakehani and A. A. Alsairafi, *Korean J. Chem. Eng.*, **27**, 1150 (2010).
15. K. M. Dhanasekharan, J. Sanyal, A. Jain and A. Haidari, *Chem. Eng. Sci.*, **60**, 213 (2005).
16. M. T. Raimondi, M. Moretti, M. Cioffi, C. Giordano, F. Boschetti, K. Lagana and R. Pietrabissa, *Biorheology*, **43**, 215 (2006).
17. V. Santos-Moreau, L. Brunet-Errard and M. Rolland, *Chem. Eng. Sci.*, **207**, 596 (2012).
18. K. A. Williams, S. Saini and T. M. Wick, *Biotechnol. Prog.*, **18**, 951 (2002).
19. M. R. Marten, K. S. Wenger and S. A. Khan, *Rheology mixing time, and regime analysis for a production-scale Aspergillus oryzae fermentation*, *in, A. W. Nienow (Ed.), Bioreactor and Bioprocess Fluid Dynamics*, BHR Group, Edinburgh (1997).
20. B. H. Um and T. R. Hanley, *Korean J. Chem. Eng.*, **25**, 1094 (2008).
21. V. V. Ranade, J. R. Bourne and J. B. Joshi, *Chem. Eng. Sci.*, **46**, 1883 (1991).
22. J. Y. Xia, S. J. Wang, S. L. Zhang and J. J. Zhong, *Biochem. Eng. J.*, **38**, 406 (2007).
23. F. F. Garcia-Ochoa and E. Gomez, *Chem. Eng. Sci.*, **59**, 2489 (2004).
24. J. Y. Xia, S. J. Wang, S. L. Liang and J. J. Zhong, *Biochem. Eng. J.*, **38**, 406 (2008).
25. T. Kumaresan and J. B. Joshi, *Chem. Eng. J.*, **115**, 173 (2006).
26. V. Abrardi, G. Rovero, G. Baldi, S. Sicardi and R. Conti, *Chem. Eng. Res. Des.*, **68**, 516 (1990).
27. S. U. Ahmed, P. Ranganathan, A. Pandey and S. Sivaraman, *J. Biosci. Bioeng.*, **6**, 588 (2010).
28. C. Tollnick, G. Seidel, M. Beyer and K. Schgüerl, *Adv. Biochem. Eng. Biotechnol.*, **86**, 1 (2004).
29. S. J. Chiang, *J. Ind. Microbiol. Biotechnol.*, **31**, 99 (2004).
30. R. P. Elander, *Appl. Microbiol. Technol.*, **61**, 385 (2003).
31. J. H. Kim, J. S. Lim, C. H. Kim and S. W. Kim, *Lett. Appl. Microbiol.*, **40**, 307 (2005).
32. M. Matsumura, T. Imanaka, T. Yoshida and H. Taguchi, *J. Ferment. Technol.*, **58**, 197 (1980).
33. S. Basak, A. Velayudhan and M. R. Ladisch, *Biotechnol. Prog.*, **11**, 626 (1995).